



Article

Strengthened Optical Nonlinearity of V₂C Hybrids Inlaid with Silver Nanoparticles

Yabin Shao ¹, Qing He ², Lingling Xiang ¹, Zibin Xu ¹, Xiaou Cai ¹ and Chen Chen ^{3,*}

¹ School of Jia Yang, Zhejiang Shuren University, Shaoxing 312028, China; shao_yabin@163.com (Y.S.); melody.xiang@vip.163.com (L.X.); xu_zibin@163.com (Z.X.); cai.xo@163.com (X.C.)

² Collaborative Innovation Center of Steel Technology, University of Science and Technology Beijing, Beijing 100083, China; 123simon@163.com

³ College of Civil Engineering, East University of Heilongjiang, Harbin 150086, China

* Correspondence: chen_chen1600@163.com

Abstract: The investigation of nonlinear optical characteristics resulting from the light–matter interactions of two-dimensional (2D) nano materials has contributed to the extensive use of photonics. In this study, we synthesize a 2D MXene (V₂C) monolayer nanosheet by the selective etching of Al from V₂AlC at room temperature and use the nanosecond Z-scan technique with 532 nm to determine the nonlinear optical characters of the Ag@V₂C hybrid. The z-scan experiment reveals that Ag@V₂C hybrids usually exhibits saturable absorption owing to the bleaching of the ground state plasma, and the switch from saturable absorption to reverse saturable absorption takes place. The findings demonstrate that Ag@V₂C has optical nonlinear characters. The quantitative data of the nonlinear absorption of Ag@V₂C varies with the wavelength and the reverse saturable absorption results from the two-photon absorption, which proves that Ag@V₂C hybrids have great potential for future ultrathin optoelectronic devices.

Keywords: Ag@V₂C MXene; hybrids; Z-scan; nonlinear optical properties



Citation: Shao, Y.; He, Q.; Xiang, L.; Xu, Z.; Cai, X.; Chen, C. Strengthened Optical Nonlinearity of V₂C Hybrids Inlaid with Silver Nanoparticles. *Nanomaterials* **2022**, *12*, 1647. <https://doi.org/10.3390/nano12101647>

Academic Editor: Eric Waclawik

Received: 8 March 2022

Accepted: 6 May 2022

Published: 12 May 2022

Publisher's Note: MDPI stays neutral with regard to jurisdictional claims in published maps and institutional affiliations.



Copyright: © 2022 by the authors. Licensee MDPI, Basel, Switzerland. This article is an open access article distributed under the terms and conditions of the Creative Commons Attribution (CC BY) license (<https://creativecommons.org/licenses/by/4.0/>).

1. Introduction

MXenes [1], 2D transition metal carbides and nitrides, exhibit the outstanding advantages of electrical conductivity, a beneficial elastic modulus and capacitance, an adaptable band gap and optical transparency [2–6]. Nonlinear optical (NLO) properties of MXene have drawn wide attention [7]. Among them, Ti₃C₂T_x is the first and most-studied MXene, and the research has been progressing vigorously regarding the linear optical properties [8–13].

Ti₃C₂T_x thin films was studied by Mochalin and Podila et al., and the findings exhibited a high modulation depth of 50% and high damage thresholds of 70 mJ cm^{−2} [11]. Ti₃C₂T_x was synthesized by Wen and Zhang et al. who revealed the Ti₃C₂T_x maximum nonlinear absorption coefficient 10–21 m²/V² had been increased tremendously compared with other 2D materials [12].

Thus far, the linear optical properties have been explored experimentally and theoretically in an extensive way, while little attention has been drawn to V₂CT_x's optical nonlinear features as well as its related applications. The Z-scan technique proposed by Sheik-Bahae et al. is simple and accurate and is widely used to study the nonlinear properties of materials (particularly non-fluorescent) [13].

To achieve the application-oriented demands for MXenes, a large variety of modified techniques have been invented to obtain desired functionalities, such as the previous studies on colloidal solutions of nanoparticles (NPs) hybridized by graphene, TMDs, etc. [14].

Moreover, great breakthroughs have taken place in NLO applications via hybridizing NPs in the past few years in accordance with their defect states, surface control and excellent plasmonic properties [15–17]. In various experiments on its broadband and strong NLO response, V₂CT_x nanosheets, a new member of the MXene family, has drawn extensive

attention due to its novel optical properties. Recent studies have shown that it has very good performance in hybrid mode-locking and good optical nonlinear properties, which indicates its good potential applications in acting as sensors and nonlinear components for lasers [18,19].

2. Materials and Methods

2.1. Preparation of Ag@V₂C Hybrids

First, 400 mesh V₂AlC (1 g) powder (Suzhou Beike Nano Technology Co., Ltd., Suzhou, China) is added slowly to 50% (v/v) HF solution, and it is stirred at room temperature for 90 h [16–18] to ensure the V-Al bonds are completely disconnected from V₂AlC with the V-C bonds intact. Second, to stratify the V₂CT_x, 30 mL tetraethylammonium hydroxide (TMAOH 25% in H₂O) is blended with 1 g multilayer V₂CT_x and sonicated for 30 min at room temperature, and the precipitates are rinsed with deionized water to neutrality (pH ≥ 6). Then, the excess TMAOH is discarded from the product by repeated centrifugation at 3000 rpm. Finally, a 2D monolayer V₂CT_x MXene material is obtained via freeze-drying.

The Ag@V₂C hybrids are made ready by mingling the V₂C hybrid dispersion and AgNO₃ solution. These are shown in Figure 1. First, 3 mL of original V₂C colloidal solution (1 mg/mL) in 30 mL of AgNO₃ solution (1 mg/mL) is re-dispersed, and the mixture is sonicated for 30 min. Then, the obtained colloidal solution of hybrid nanocomposites of Ag@V₂C hybrids is centrifuged at 12,000 rpm for 20 min and re-dispersed in 30 mL deionized water.

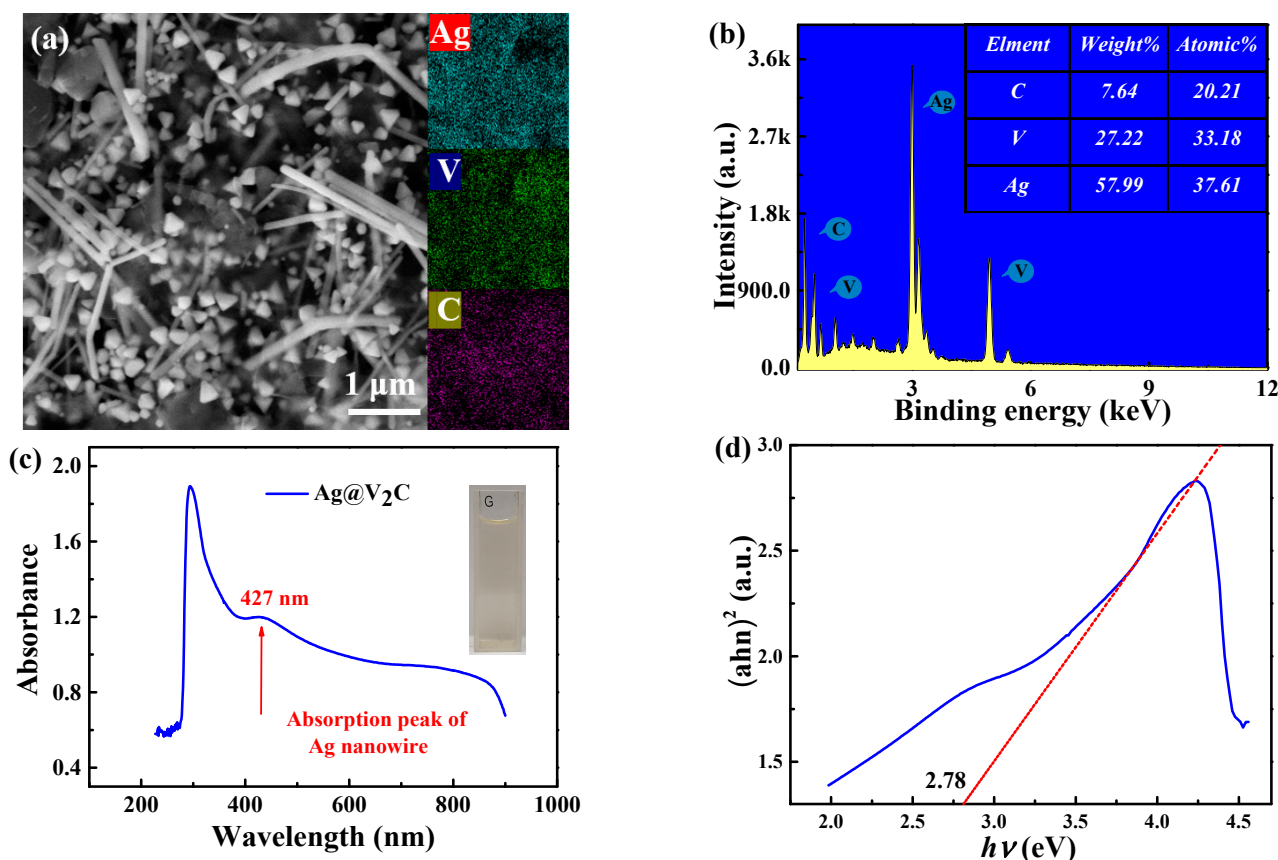


Figure 1. (a) SEM and EDS mappings of Ag V C elements. (b) EDS of Ag@V₂C. The inset is atomic ratios for diverse elements. (c) Optical absorption spectra of Ag@V₂C. (d) Estimation of the band gap of Ag@V₂C.

2.2. Optical Experimental Setup

SEM on a ZEISS Sigma 300 (acceleration voltage: 15 kV, Dublin, CA, USA) was employed to perform the morphological study with a spectrometer (Ocean Optics 4000, CA, USA) to survey the UV–Vis–NIR spectra of monolayer V_2CT_x MXene. To evaluate the NLO features of V_2CT_x MXene flakes nanoparticles, we performed an experiment of a single beam open aperture (OA) Z-scan, with the help of a 6 ns 8 Hz Q-switched Nd:YAG nanosecond pulse laser (Surelite II, Continuum, San Jose, CA, USA) and an optical parametric oscillator (Continuum, APE OPO) to produce lasers beams of diverse wavelengths. In this experiment, the linear transmittance of the V_2CT_x hybrids solution was measured at 500 nm wavelength, and we found that it was 72%.

The laser beam with a waist diameter of 200 μm is focused through a lens with a focal length of 20 cm and projected onto a 2 mm diameter quartz cuvette filled with aqueous dispersion of V_2CT_x monolayer flake nanoparticles. The cuvette is installed on a computer-operated translation motion stage where the transmitted data for every z point is recorded by stored program. Their NLO properties are studied by Z-scan technology under 532 nm nanosecond laser pulses. The findings indicate that the $Ag@V_2CT_x$ has a large nonlinear absorption coefficient.

3. Results

Figure 1a illustrates the typically morphologic multilayer $Ag@V_2C$ with coarse surface and the shape of accordion. The elements mapping data of SEM in combination with EDS illustrates that the Ag, V and C elements are evenly dispersed in the monolayer V_2C . In Figure 1b, the fundamental analysis of $Ag@V_2C$ V_2C , the result of C: V: Ag \approx 2:3:3 is obtained via the energy dispersive X-ray energy spectrum (EDS), while it is impracticable to measure the content of other elements by EDS due to the inadequate content.

In Figure 1c, the linear absorbance spectra of $Ag@V_2C$ is investigated by using ultraviolet visible near infrared spectrophotometer to observe two absorption peaks—that is, 315 and 427 nm. These findings justify that the surface of $Ag@V_2C$ is functionalized with Ag nanoparticles, and the positions of the peaks were predicted by theoretical calculations. In Figure 1d, the estimated band gap value of $Ag@V_2C$ is 2.75~2.80 eV according to Kubelka-Munk's theory in previous data [19].

Hereinafter are the three different phases. In Figure 2a, the transmittance of $Ag@V_2C$ hybrids remains flat before rising sharply when the Z position approaches zero, and a peak is observed, which reflects the SA property. In Figure 2b, the conversion from SA to RSA is observed. The transmittance goes up to the first peak to indicate SA property and then falls back to a valley to indicate the reverse saturable absorption RSA property when the Z position approaches zero. It then rises again to the second peak and falls back to the flat linear transmittance. In Figure 2c, the laser pulse energy mounts to 681 when a deep valley occurs, which indicates the RSA property. Figure 2a–c, in general, reveals a whole process of NLO properties, including SA, conversion and RSA.

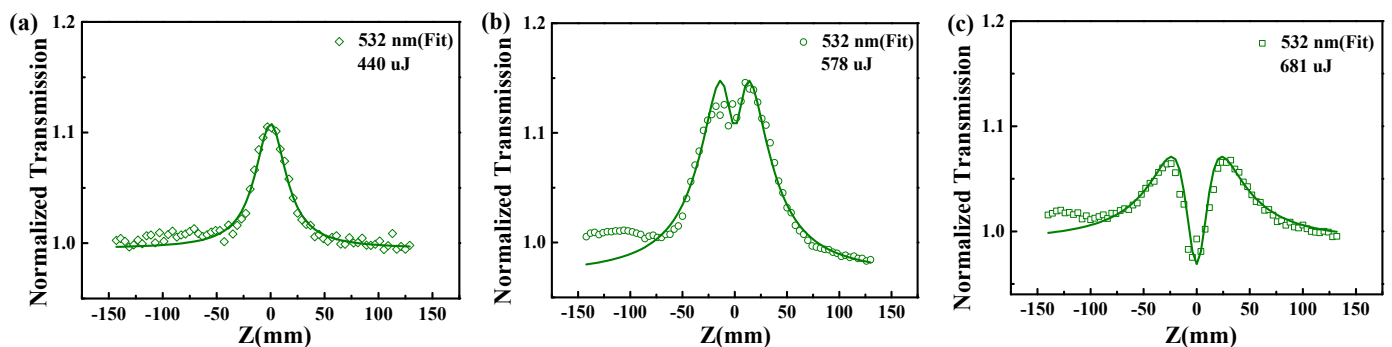


Figure 2. Open aperture Z-scan is conducted at the wavelength of 532 nm and the laser energies at (a) 440 μJ , (b) 578 μJ and (c) 681 μJ to obtain the normalized transmission of V_2CT_x hybrid colloid.

The physical mechanism of NLO properties can be expounded as follows in Figure 3. The above findings are related in the main to the changing energy of incident laser pulse and the nature property of MXene. It is generally believed that nonlinear susceptibility of the material results from intraband transition, interband transition, hot electron excitation and thermal effects. [20]. Specifically, when Ag@V₂C monolayer flakes are at low pulse energy, one photon absorption arises to indicate the SA property [21].

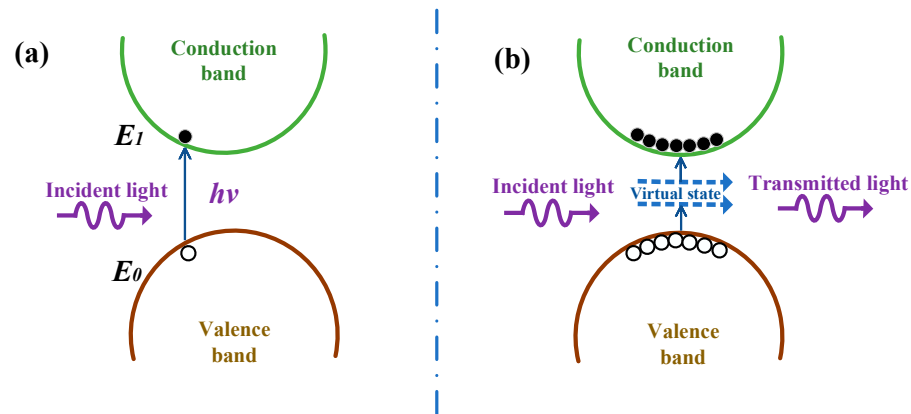


Figure 3. The physical mechanism of the NLO properties of Ag@V₂C monolayer flakes. (a) One photon absorption. (b) Two photon absorption.

Under laser irradiance, as the sample approaches the focal point, the laser energy increases abruptly, and the materials absorbs much incident light pulse when Ag@V₂C monolayer hybrids are pumped into an excited state, leaving a small amount at the ground state. Thus, more light penetrates the sample to make the transmittance higher and SA can be observed [22]. This phenomenon is termed ground-state bleaching of the plasmon band.

To remove the thermal effect's influence on the possibility of nonlinearity, a laser pulse was set with a short duration and low repetition rate (10 Hz and 6 ns). Moreover, as the incident pulse energy goes up to 1080 μJ, the conversion appears; as it reaches 1380 μJ, RSA occurs. The major causes of RSA may be due to the excited state absorption (ESA) and two-photon absorption (TPA) [23].

The quantitative findings of the Z-scan experiment are as follows. The quantitative relationship between laser energy intensity and optical path length can be expressed as follows [24]:

$$dI = -\alpha I dz \quad (1)$$

In Equation (1), I signifies the laser intensity, z signifies the optical path length, and α signifies the absorption coefficient. The absorption coefficient combining SA and RSA in Ag@V₂C monolayer hybrids is expressed in Equation (2) [25]:

$$\alpha(I) = \frac{\alpha_0}{1 + (I/I_s)} + \beta I \quad (2)$$

Here, α_0 signifies the linear absorption coefficient of Ag@V₂C monolayer hybrids, I signifies the laser intensity, I_s is the saturable intensity, and β is the positive nonlinear absorption coefficient. I in Equation (3) can also be expressed as follows in Equation (3):

$$I = \frac{I_0}{1 + z^2/z_0^2} \quad (3)$$

Therefore, Equation (2) can be reconsidered as:

$$\alpha(I_0) = \frac{\alpha_0}{1 + \frac{I_0}{(1+z^2/z_0^2)I_s}} + \frac{\beta I_0}{1 + z^2/z_0^2} \quad (4)$$

With the help of Equations (1)–(4), the data of normalized transmission in Figure 3 can be fitted. In this way, related parameters are obtained as shown in Table 1.

Table 1. The nonlinear optical parameters of Ag@V₂C monolayer flake hybrids.

λ (nm)	I_0 (W/m ²)	I_s (W/m ²)	β (m/W)
532	1.1×10^{14}	0.61×10^6	-
	1.4×10^{14}	0.82×10^6	
	7.4×10^{13}	0.23×10^6	
			1.12×10^{-10}

To inspect the ultrafast carrier dynamics of Ag@V₂C hybrids, broadband transient absorption was studied. In Figure 4a, TA spectra of Ag@V₂C hybrids are illustrated by 2D map of TA signals that have been achieved temporally and spectrally. A constant pump fluence (6.4×10^3 mW/cm²) and probe beam ranging from 450 to 600 nm are employed to measure broadband TA signals and obtain the 2D color coded maps, cut horizontally through each map five times to obtain five differential absorption spectra at different delay times (0, 3.2, 4.0, 6.6 and 11 ps).

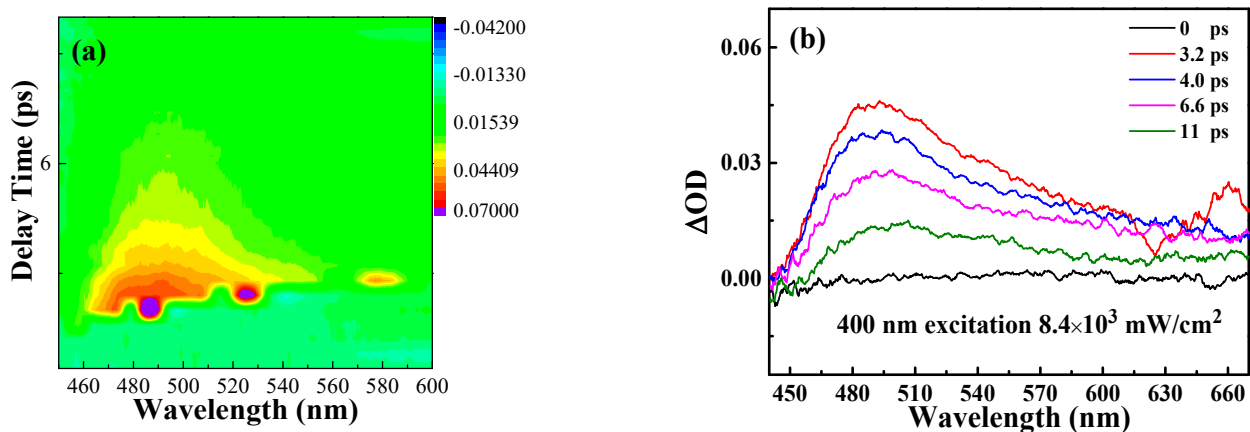


Figure 4. Carrier dynamics (at 400 nm pump) curves for Ag@V₂C. (a) Two-dimensional (2D) mapping of transient absorption spectra pumped at 400 nm with a fluence of 8.4×10^3 mW/cm², (b) Time and wavelength resolved transient absorption data of Ag@V₂C.

In Figure 4b, a positive absorption proves the generation of excited state absorption (ESA) in the spectral region as well as an ultrafast carrier relaxation process within the scale of ps. When the delay time increases, the amplitude of TA spectrum is reduced. The black curve, around the 0 ps delay time, signifies the unexcited Ag@V₂C hybrids. The peak value of Ag@V₂C hybrids, 485 nm, forms when the photo-induced absorption is brought about by the conversion of occupied–unoccupied states, which are found in the Z-scan experiment as RSA [26–28].

Then, the TA signal decays at ~13 ps and falls back to zero in the full waveband. The energy of the pump light markedly exceeds the energy bandgap of the Ag@V₂C nanosheet, the former 400 nm (~3.10 eV) laser, the latter being ~2.78 eV). Hence, with the incident laser pulse working up, electrons are excited and jump back and forth to the conduction band, while the holes remain in the valence band [29].

Soon afterwards is the conversion from electrons to hot electrons through photo-exciting with Fermi–Dirac distribution. The hot carriers will chill down shortly in sync with the decay process through e–e and e–ph diffusion on the conduction band, and with the carrier-phonon dispersing over a few relaxation processes, the hot carriers relax from the conduction band to the valence band and reunite with the holes.

In Figure 5a, the carrier dynamics are inspected at various wavelengths—that is, 480, 495, 515 and 540 nm, as shown in the figure. The optical transmission responses of Ag@V₂C hybrids are composed of two decay processes, a fast and a slow one. Coulomb-induced

hot electrons are excited to be at the core state and be trapped by the surface state before releasing spare energy by dispersing the optical phonons (3.9 ps). The rest of the chilled electrons will experience nonradiative transition to fall back to ground state within 30.1 ps [30,31]. The above-mentioned biexponential decay function is formulated in Equation (3) [32].

$$\frac{\Delta T}{T} = A_1 \exp\left(-\frac{t}{\tau_1}\right) + A_2 \exp\left(-\frac{t}{\tau_2}\right) \quad (5)$$

where A_1 and A_2 signify the amplitudes of the fast, slow decay components, respectively; and τ_1 and τ_2 are the decay lifetimes of each component, correspondingly. The experimental data in Figure 5a justify the formulation of Equation (3) through which the fast and slow decay components, τ_1 and τ_2 , are determined along with the rise of probe wavelengths owing to electrons at the lower energy states that are more apt to be detected and whose number is less likely to decrease than those at higher energy states. Similar properties can be seen in graphite [33].

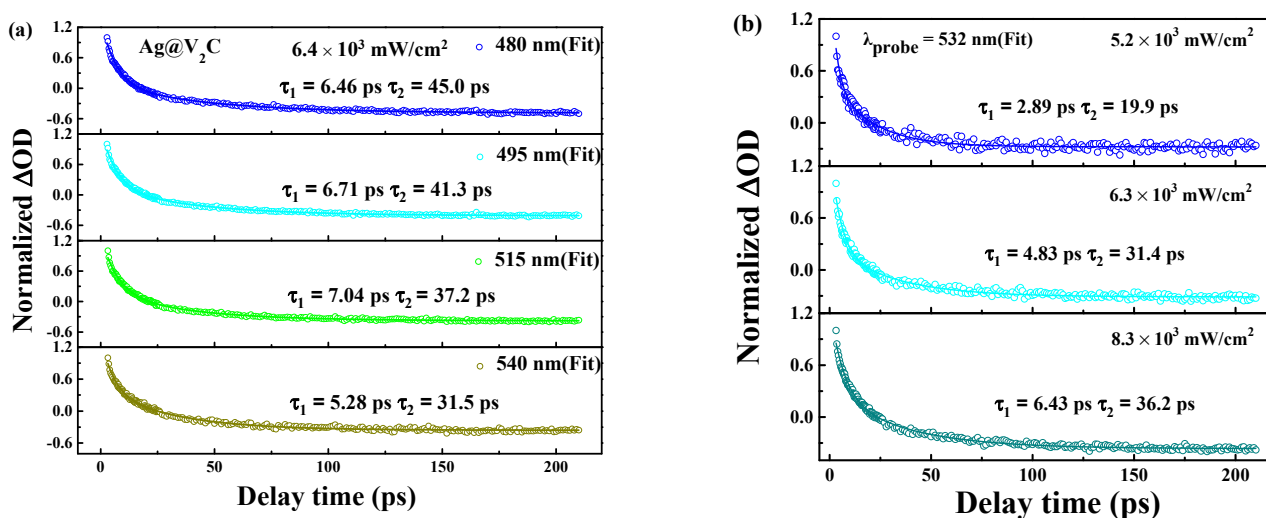


Figure 5. (a) Carrier dynamics (at 400 nm pump) curves for Ag@V₂C nanosheet at various probe wavelengths of 480, 495, 525, 515 and 540 nm, respectively. The scatters are experimental data while the solid lines are theoretical fit generated with pump fluence fixed at 6.4×10^3 mW/cm². (b) Carrier dynamics curves (at 400 nm pump) at different pump fluences 5.2×10^3 , 6.3×10^3 and 8.3×10^3 mW/cm² with a probe wavelength fixed at 532 nm.

The pump fluence effect on carrier dynamics is inspected at the 500 nm probe wavelength. In Figure 5b, the findings of various pump-fluences (5.1×10^3 , 6.4×10^3 and 8.1×10^3 mW/cm²) accord with the results by applying Equation (3) and the corresponding parameters. With the rise of pump fluence, τ_1 goes up from 3.9 to 4.5 ps, and τ_2 goes from 11.1 to 13.2 ps, which is inseparable to the carrier density and its reliance on e–ph coupling [34]).

In brief, the faster decay part of 2D materials follow the principle of e–ph scattering, while the slower part that of ph–ph scattering [35], among which the necessary basis of the electrons’ energy transfer is the electron–phonon interaction [36]. Ultimately, the improved efficiency of electron–phonon interaction promotes the cooling process, or in other words, it is high energy injection that speeds up electron decay. Similar properties can be seen in either quantum dots or 2D films [37–39].

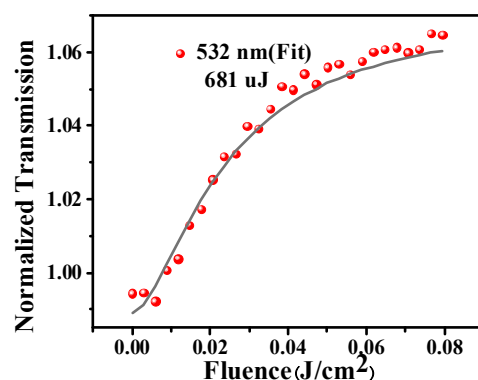
The data shown in Figure 5 can be verified upon checking Equation (3) and please see in Table 2 regarding τ_1 and τ_2 .

Table 2. Carrier dynamics parameters of the Ag@V₂C nanosheet.

	λ (nm)	τ_1 (ps)	τ_2 (ps)
Ag@V ₂ C	470	4.5	33.9
	485	4.6	36.5
	500	4.2	43.1
	520	3.9	45.8
V ₂ C nanosheet	470	3.8	18.0
	485	3.2	27.4
	500	4.6	22.5
	520	4.6	19.9

Resulting from the high density of Ag, those aroused electrons in the CB of Ag@V₂C hybrids tend to move to the d band of Ag atoms until the bleaching effect of VB disappears, which extends the aroused, composite electrons' lifetime and, accordingly, leads to more violent RSA properties [40]. Next, the electrons in the d band become excited functional groups to take in incident light before they move to a higher energy level and lead to an improved RSA effect. Then, the carriers that are excited and dressed with Ag nanoparticles will move from CB of Ti₃C₂ to the sp band of the metal until they reach VB of Ag@V₂C hybrids. Compared with direct decay of pure Ti₃C₂ nanosheet, this takes a longer time scale (50 ps), and thus it enhances the RSA performance. Similar properties can be seen in other 2D materials [41].

Figure 6 exhibits the optical limiting response at 532 nm. With the increase of incident energy, the transmittance increases rapidly at first. When the incident energy continues to increase, the transmittance does not change drastically, which indicates that Ag@V₂C has superior optical limiting ability and can be used to manufacture optical limiting devices.

**Figure 6.** The optical limiting response at 532 nm.

4. Conclusions

Ag@V₂C ultrathin hybrids were synthesized via conventional etching, and remarkable NLO properties of Ag@V₂C hybrids were found through the OA z-scan technique at 532 nm. SA and RSA properties resulted mainly from GSB and TPA. Moreover, femtosecond transient absorption spectroscopy was adopted to inspect the ultrafast dynamics of the specimen, and we found that its decay contained a fast decay component (~4.5 ps) resulting from electron–phonon interactions and a slow component (~40 ps) from phonon–phonon interactions. Additionally, the two decay times increased with the pump fluence. The experiments confirmed that Ag@V₂C hybrids can be used in ultrafast optoelectronics and optical limiters.

Author Contributions: Data curation, C.C.; Funding acquisition, L.X., Z.X. and X.C.; Investigation, Y.S.; Resources, Q.H.; Writing—review and editing, L.X. All authors have read and agreed to the published version of the manuscript.

Funding: The article was supported by the following funds, Natural Science Foundation of Heilongjiang Province (Grant No. LH2021A019), East University of Heilongjiang Scientific Research Fund (Grant Nos. HDFHX210110, 210111, HDFKYTD202105) and Scientific research fund of Zhejiang Shuren University (Grant No. 2021R037).

Institutional Review Board Statement: Not applicable.

Informed Consent Statement: Not applicable.

Data Availability Statement: Data sharing is not applicable to this article.

Conflicts of Interest: The authors declare no conflict of interest.

References

1. Naguib, M.; Kurtoglu, M.; Presser, V.; Lu, J.; Niu, J.; Heon, M.; Hultman, L.; Gogotsi, Y.; Barsoum, M.W. Two-dimensional nanocrystals produced by exfoliation of Ti_3AlC_2 . *Adv. Mater.* **2011**, *23*, 4248–4253. [[CrossRef](#)] [[PubMed](#)]
2. Keller, U. Recent developments in compact ultrafast lasers. *Nature* **2003**, *424*, 831–838. [[CrossRef](#)] [[PubMed](#)]
3. Mashtalir, O.; Naguib, M.; Mochalin, V.N.; Dall’Agnese, Y.; Heon, M.; Barsoum, M.W.; Gogotsi, Y. Intercalation and delamination of layered carbides and carbonitrides. *Nat. Commun.* **2013**, *4*, 1716. [[CrossRef](#)] [[PubMed](#)]
4. Lukatskaya, M.R.; Mashtalir, O.; Ren, C.E.; Dall’Agnese, Y.; Rozier, P.; Taberna, P.L.; Naguib, M.; Simon, P.; Barsoum, M.W.; Gogotsi, Y. Cation intercalation and high volumetric capacitance of two-dimensional titanium carbide. *Science* **2013**, *341*, 1502–1505. [[CrossRef](#)] [[PubMed](#)]
5. Shahzad, F.; Alhabeab, M.; Hatter, C.B.; Anasori, B.; Hong, S.M.; Koo, C.M.; Gogotsi, Y. Electromagnetic interference shielding with 2D transition metal carbides (MXenes). *Science* **2016**, *353*, 1137–1140. [[CrossRef](#)]
6. Peng, Q.; Guo, J.; Zhang, Q.; Xiang, J.; Liu, B.; Zhou, A.; Liu, R.; Tian, Y. Unique lead adsorption behavior of activated hydroxyl group in two-dimensional titanium carbide. *J. Am. Chem. Soc.* **2014**, *136*, 4113–4116. [[CrossRef](#)]
7. Jhon, Y.L.; Koo, J.; Anasori, B.; Seo, M.; Lee, J.H.; Gogotsi, Y.; Jhon, Y.M. Metallic MXene Saturable Absorber for Femtosecond Mode-Locked Lasers. *Adv. Mater.* **2017**, *29*, 1702496–1702503. [[CrossRef](#)]
8. Enyashin, A.; Ivanovskii, A. Two-dimensional titanium carbonitrides and their hydroxylated derivatives: Structural, electronic properties and stability of MXenes $\text{Ti}_3\text{C}_{2-x}\text{N}_x(\text{OH})_2$ from DFTB calculations. *J. Solid State Chem.* **2013**, *207*, 42–48. [[CrossRef](#)]
9. Lashgari, H.; Abolhassani, M.; Boocheani, A.; Elahi, S.; Khodadadi, J. Electronic and optical properties of 2D graphene-like compounds titanium carbides and nitrides: DFT calculations. *Solid State Commun.* **2014**, *195*, 61–69. [[CrossRef](#)]
10. Mauchamp, V.; Bugnet, M.; Bellido, E.P.; Botton, G.A.; Moreau, P.; Magne, D.; Naguib, M.; Cabioch, T.; Barsoum, M.W. Enhanced and tunable surface plasmons in two-dimensional Ti_3C_2 stacks: Electronic structure versus boundary effects. *Phys. Rev. B* **2014**, *89*, 235428. [[CrossRef](#)]
11. Berdiyrov, G. Optical properties of functionalized $\text{Ti}_3\text{C}_2\text{T}_2$ (T=F, O, OH) MXene: First-principles calculations. *AIP Adv.* **2016**, *6*, 055105. [[CrossRef](#)]
12. Hantanasirisakul, K.; Zhao, M.Q.; Urbankowski, P.; Halim, J.; Anasori, B.; Kota, S.; Ren, C.E.; Barsoum, M.W.; Gogotsi, Y. Fabrication of $\text{Ti}_3\text{C}_2\text{T}_x$ MXene transparent thin films with tunable optoelectronic properties. *Adv. Electron. Mater.* **2016**, *2*, 1600050. [[CrossRef](#)]
13. Dillon, A.D.; Ghidui, M.J.; Krick, A.L.; Griggs, J.; May, S.J.; Gogotsi, Y.; Barsoum, M.W.; Fafarman, A.T. Highly conductive optical quality solution-processed films of 2D titanium carbide. *Adv. Funct. Mater.* **2016**, *26*, 4162–4168. [[CrossRef](#)]
14. Kim, I.Y.; Jo, Y.K.; Lee, J.M.; Wang, L.; Hwang, S.-J. Unique Advantages of Exfoliated 2D Nanosheets for Tailoring the Functionalities of Nanocomposites. *J. Phys. Chem. Lett.* **2014**, *5*, 4149–4161. [[CrossRef](#)] [[PubMed](#)]
15. Biswas, S.; Kole, A.K.; Tiwary, C.S.; Kumbhakar, P. Enhanced nonlinear optical properties of graphene oxide–silver nanocomposites measured by Z-scan technique. *RSC Adv.* **2016**, *6*, 10319–10325. [[CrossRef](#)]
16. Li, Z.; Dong, N.; Cheng, C.; Xu, L.; Chen, M.; Wang, J.; Chen, F. Enhanced nonlinear optical response of graphene by silver-based nanoparticle modification for pulsed lasing. *Opt. Mater. Express* **2018**, *8*, 1368–1377. [[CrossRef](#)]
17. Yan, X.; Wu, X.; Fang, Y.; Sun, W.; Yao, C.; Wang, Y.; Zhang, X.; Song, Y. Effect of silver doping on ultrafast broadband nonlinear optical responses in polycrystalline Ag-doped InSe nanofilms at near-infrared. *RSC Adv.* **2020**, *10*, 2959–2966. [[CrossRef](#)]
18. Ma, C.Y.; Huang, W.C.; Wang, Y.Z.; Adams, J.; Wang, Z.H.; Liu, J.; Song, Y.F.; Ge, Y.Q.; Guo, Z.Y.; Hu, L.P.; et al. MXene saturable absorber enabled hybrid mode-locking technology: A new routine of advancing femtosecond fiber lasers performance. *Nanophotonics* **2020**, *9*, 2451–2458. [[CrossRef](#)]
19. He, Q.; Hu, H.H.; Shao, Y.B.; Zhao, Z.Z. Switchable optical nonlinear properties of monolayer V_2CT_x MXene. *Optik* **2021**, *247*, 167629. [[CrossRef](#)]
20. Naguib, M.; Gogotsi, Y. Synthesis of Two-Dimensional Materials by Selective Extraction. *Acc. Chem. Res.* **2015**, *48*, 128–135. [[CrossRef](#)]
21. Jiang, X.; Liu, S.; Liang, W.; Luo, S.; He, Z.; Ge, Y.; Wang, H.; Cao, R.; Zhang, F.; Wen, Q. Broadband nonlinear photonics in few-layer MXene $\text{Ti}_3\text{C}_2\text{T}_x$ (T=F, O, or OH). *Laser Photonics Rev.* **2018**, *12*, 1700229. [[CrossRef](#)]
22. Dong, Y.; Chertopalov, S.; Maleski, K.; Anasori, B.; Hu, L.; Bhattacharya, S.; Rao, A.M.; Gogotsi, Y.; Mochalin, V.N.; Podila, R. Saturable absorption in 2D Ti_3C_2 MXene thin films for passive photonic diodes. *Adv. Mater.* **2018**, *30*, 1705714. [[CrossRef](#)] [[PubMed](#)]

23. Wang, J.; Chen, Y.; Li, R.; Dong, H.; Zhang, L.; Lotya, M.; Coleman, J.N.; Blau, W.J. Nonlinear optical properties of graphene and carbon nanotube composites. In *Carbon Nanotubes-Synthesis, Characterization, Applications*; Yellampalli, S., Ed.; IntechOpen: London, UK, 2011.
24. Sheik-Bahae, M.; Said, A.A.; Wei, T.; Hagan, D.J.; Stryland, E.W.V. Sensitive measurement of optical nonlinearities using a single beam. *IEEE J. Quantum Electron.* **1990**, *26*, 760–769. [[CrossRef](#)]
25. Wu, W.; Chai, Z.; Gao, Y.; Kong, D.; Wang, Y. Carrier dynamics and optical nonlinearity of alloyed CdSeTe quantum dots in glass matrix. *Opt. Mater. Express* **2017**, *7*, 1547–1556. [[CrossRef](#)]
26. Wang, J.; Ding, T.; Wu, K. Charge transfer from n-doped nanocrystals: Mimicking intermediate events in multielectron photocatalysis. *J. Am. Chem. Soc.* **2018**, *140*, 7791–7794. [[CrossRef](#)]
27. Lu, S.; Sui, L.; Liu, Y.; Yong, X.; Xiao, G.; Yuan, K.; Liu, Z.; Liu, B.; Zou, B.; Yang, B. White Photoluminescent Ti₃C₂ MXene Quantum Dots with Two-Photon Fluorescence. *Adv. Sci.* **2019**, *6*, 1801470. [[CrossRef](#)]
28. Wu, K.; Chen, J.; McBride, J.R.; Lian, T. Efficient hot-electron transfer by a plasmon-induced interfacial charge-transfer transition. *Science* **2015**, *349*, 632–635. [[CrossRef](#)]
29. Xie, Z.; Zhang, F.; Liang, Z.; Fan, T.; Li, Z.; Jiang, X.; Chen, H.; Li, J.; Zhang, H. Revealing of the ultrafast third-order nonlinear optical response and enabled photonic application in two-dimensional tin sulfide. *Photonics Res.* **2019**, *7*, 494–502. [[CrossRef](#)]
30. Zhang, H. Ultrathin Two-Dimensional Nanomaterials. *ACS Nano* **2015**, *10*, 9451–9469. [[CrossRef](#)]
31. Wibmer, L.; Lages, S.; Unruh, T.; Guldi, D.M. Excitons and Trions in One-Photon- and Two-Photon-Excited MoS₂: A Study in Dispersions. *Adv. Mater.* **2018**, *30*, 1706702. [[CrossRef](#)]
32. Guo, J.; Shi, R.; Wang, R.; Wang, Y.; Zhang, F.; Wang, C.; Chen, H.; Ma, C.; Wang, Z.; Ge, Y.; et al. Graphdiyne-Polymer Nanocomposite as a Broadband and Robust Saturable Absorber for Ultrafast Photonics. *Laser Photonics Rev.* **2020**, *14*, 1900367–1900378. [[CrossRef](#)]
33. Breusing, M.; Ropers, C.; Elsaesser, T. Ultrafast Carrier Dynamics In Graphite. *Phys. Rev. Lett.* **2009**, *102*, 210–213. [[CrossRef](#)] [[PubMed](#)]
34. Xu, Y.; Jiang, X.-F.; Ge, Y.; Guo, Z.; Zeng, Z.; Xu, Q.-H.; Han, Z.; Yu, X.-F.; Fan, D. Size-dependent nonlinear optical properties of black phosphorus nanosheets and their applications in ultrafast photonics. *J. Mater. Chem. C* **2017**, *5*, 3007–3013. [[CrossRef](#)]
35. Gao, L.; Chen, H.; Zhang, F.; Mei, S.; Zhang, Y.; Bao, W.; Ma, C.; Yin, P.; Guo, J.; Jiang, X.; et al. Ultrafast Relaxation Dynamics and Nonlinear Response of Few-Layer Niobium Carbide MXene. *Small Methods* **2020**, *4*, 2000250. [[CrossRef](#)]
36. Brongersma, M.L.; Halas, N.J.; Nordlander, P. Plasmon-induced hot carrier science and technology. *Nat. Nanotechnol.* **2015**, *10*, 25–34. [[CrossRef](#)]
37. Urayama, J.; Norris, T.B.; Singh, J.; Bhattacharya, P. Observation of Phonon Bottleneck in Quantum Dot Electronic Relaxation. *Phys. Rev. Lett.* **2001**, *86*, 4930–4933. [[CrossRef](#)]
38. Wang, J.; Wu, C.; Dai, Y.; Zhao, Z.; Wang, A.; Zhang, T.; Wang, Z.L. Achieving ultrahigh triboelectric charge density for efficient energy harvesting. *Nat. Commun.* **2017**, *8*, 88. [[CrossRef](#)]
39. Kameyama, T.; Sugiura, K.; Kuwabata, S.; Okuhata, T.; Tamai, N.; Torimoto, T. Hot electron transfer in Zn–Ag–In–Te nanocrystal–methyl viologen complexes enhanced with higher-energy photon excitation. *RSC Adv.* **2020**, *10*, 16361–16365. [[CrossRef](#)]
40. Kalanoor, B.S.; Bisht, P.B.; Akbar, A.S.; Baby, T.T. Optical nonlinearity of silver-decorated graphene. *J. Opt. Soc. Am. B* **2012**, *29*, 669–675. [[CrossRef](#)]
41. Yu, Y.; Si, J.; Yan, L.; Li, M.; Hou, X. Enhanced nonlinear absorption and ultrafast carrier dynamics in graphene/gold nanoparticles nanocomposites. *Carbon* **2019**, *148*, 72–79. [[CrossRef](#)]